Chemical Engineering Journal 150 (2009) 374–384

Contents lists available at ScienceDirect

Chemical Engineering Journal

journal homepage: www.elsevier.com/locate/cej

Numerical study on the cluster flow behavior in the riser of circulating fluidized beds

Huanpeng Liu*, Huilin Lu

School of Energy Science and Engineering, Harbin Institute of Technology, Harbin 150001, China

ARTICLE INFO

Article history:
Received 30 October 2008
Received in revised form 3 January 2009
Accepted 8 January 2009

Keywords:
CFBs
Cluster
DSMC method
LES
Low-pressure zone

ABSTRACT

In this paper, the cluster flow behavior in the riser of circulating fluidized beds (CFBs) was predicted by means of the Euler–Lagrange approach. Gas turbulence was modeled by means of Large Eddy Simulation (LES). Particle collision was modeled by means of the direct simulation Monte Carlo (DSMC) method. An extended cluster identification method was used to obtain the solid concentration and velocities of clusters. The flow behavior of falling clusters in the near wall region and the up-flowing and down-flowing clusters in the core of riser were analyzed respectively. At the same time, some cluster transient flow characteristics observed in the CFBs experimental studies were obtained in present simulation. Simulated results showed that there exists a low-pressure zone between the tails of a down-flowing cluster in the core of riser and a new cluster can be formed in the near wall region and transferred from the near wall region to the core of riser under the effect of upgoing gas. Simulated results have a reasonable agreement with the previous experimental findings.

1. Introduction

One important feature of hydrodynamic behavior in circulation fluidized beds (CFBs) is the existence of clusters. A cluster is a group of particles held together as a result of hydrodynamic. They will affect the macro gas–solid flow behaviors in the reactor [1]. The study of clusters has received a great deal of attention during the last decades. For example, Van Den Moortel et al. [2] investigated the hydrodynamic characteristics of solid phase in the riser of CFBs using a phase Doppler particle analyzer (PDPA). Sharma et al. [3] investigated the effect of particle size and superficial velocity on the duration time, occurrence frequency, time-fraction of existence and solid concentration of clusters using capacitance-probe measurements in a fast-fluidized bed. Manyele et al. [4] study the cluster behavior in a high-density and high-flux CFB riser. At the same time, significant research efforts have been made to develop detailed physical models to study the complex hydrodynamics of CFBs. Many investigators have used these numerical models to study the flow behavior of cluster in the riser of CFBs and obtained some valuable findings. Broadly speaking, the simulation approaches of two-phase flow in circulating fluidized beds can be classified into Euler–Euler two-fluid model and Euler–Lagrange discrete particle trajectory model. In two-fluid model, gas and solid phases are both considered as continuous mediums, and balance equations of each phase are established to investigate the flow behavior of gas and solid phases. Tsuo and Gidaspow [5] successfully simulated the flow pattern of clusters in the CFBs by means of two-fluid model. Lu et al. [6] predicted the flow behavior of clusters in CFBs by means of a proposed cluster-based approach (CBA). In the Euler–Lagrange particle trajectory model, gas is considered as the continuous medium and the motions of particles are treated in the Lagrange coordinate by solving the motion equations. Tsuji et al. [7] verified the ability of discrete particle modeling on the simulation of the formation of clusters in CFBs and found that there exist clusters in the core region of riser of CFBs. Ouyang and Li [8] studied the effects of gas velocity, solid flow rate, and inelastic collisions on cluster formation using Euler–Lagrange simulations. Helland et al. [9,10] studied the cluster structures and the fluctuating gas–solid motion in the CFBs. Yonemura and Tanaka [11] investigated the formation of clusters in the circulating fluidized bed by means of DSMC method. Effects of physical properties of particles on the structure of particle clusters were studied numerically in a rectangular domain with periodic boundaries [12]. A numerical simulation was performed for a dispersed gas–solid flow in a vertical channel by DSMC method [13]. It is found that the flow becomes unstable and inhomogeneous as the gas velocity decreases and the solid loading increase. Although a great deal of research on particle cluster characteristics has been performed in the last decades, some flow properties of clusters are still not understood very well.

In this study the locally averaged Navier–Stokes equations of gas phase and Lagrangian type particle motion equations are simul-

* Corresponding author.
E-mail address: liuhuanpeng@hit.edu.cn (H. Liu).

1385-8947/$ – see front matter © 2009 Elsevier B.V. All rights reserved.
doi:10.1016/j.cej.2009.01.015

Nomenclature

C_d	drag coefficient
d	particle diameter
e	restitution coefficient of particles
e_w	restitution of wall
g	gravity
g_0	redial distribution function
H	bed height
n	normal direction
N	the number of cluster occurrence
P	pressure
Re	Reynolds number
r	radial direction
t	tangential direction
μ_g	gas velocity
v_s	particle velocity
v_{cl}	cluster velocity
W	bed width

Greek letters

τ_g	gas stress tensor
τ_s	particle stress tensor
μ_g	gas viscosity
ε_g	void fraction
ε_{cl}	solid concentration of cluster
ρ_g	gas density
ρ_s	particle density

taneously solved. The mutual interaction between gas phase and particles is taken into account. Particle collision is modeled by means of the DSMC method. The variations of the mean velocity and solid concentration of clusters near the wall region and in the core of riser along the height of riser are analyzed respectively. The shape, occurrence frequency and existence time fraction of up-flowing and down-flowing clusters in the core of riser are compared. Some micro-scale transient flow characteristics of clusters are investigated in this study.

2. Eulerian–Lagrangian gas–solid flow model

2.1. Continuity and momentum equations for gas phase

The Euler–Lagrangian method computes the Navier–Stokes equation for the gas phase and the motion of individual particles by the Newtonian equations of motion. For the gas phase, we write the equations of conservation of mass and momentum [14]:

$$\frac{\partial}{\partial t}(\rho_g \varepsilon_g) + \nabla \cdot (\rho_g \varepsilon_g u_g) = 0 \tag{1}$$

$$\frac{\partial}{\partial t}(\varepsilon_g \rho_g u_g) + \nabla \cdot (\varepsilon_g \rho_g u_g u_g) = -\varepsilon_g \nabla P - S_{p-g} - \varepsilon_g (\nabla \cdot \tau_g) + \varepsilon_g \rho_g g \tag{2}$$

$$\tau_g = \mu_g [\nabla u_g + \nabla u_g^T] - \frac{2}{3}\mu_g \nabla \cdot u_g I \tag{3}$$

$$\mu_g = \mu_{lam,g} + \mu_t \tag{4}$$

where u_g and ρ_g are gas velocity and density, respectively. ε_g is the void fraction. The interaction forces between the two phases should be equal and have reserve directions. The value can be determined

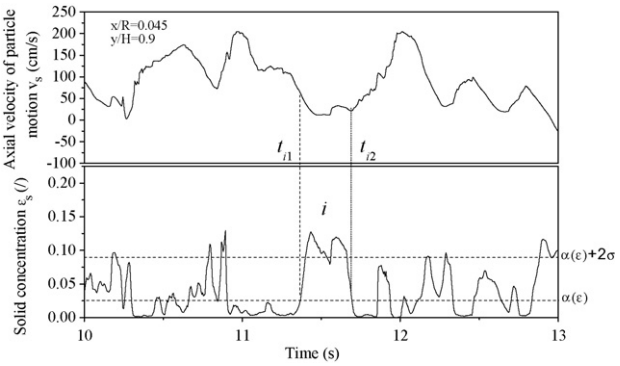

Fig. 1. Cluster identification method.

by:

$$S_{p-g} = \frac{\sum_{i=1}^{N} f_{d,i}}{S} \tag{5}$$

where $f_{d,i}$ is the interaction drag force acting on a particle.

Yuu et al. [15] has modeled turbulent viscosity coefficient of subgrid-scale turbulence caused by subgrid-scale fluctuations using LES in which the effect of particle oscillations on gas turbulence has been taken into account. The turbulent viscosity of gases is as follows:

$$\mu_t = C_V \Delta \rho_g k_g^{1/2} \tag{6}$$

where $\Delta = (xyz)^{1/2}$,and $k_g = (1/2)(\bar{u}'_{gx}\bar{u}'_{gy})$ is gas turbulent energy.

2.2. Particle motion equation

The particle motion is subjected to Newton's equation of motion. Magnus force, Saffman force, Basset, and the unsteady force are neglected due to the high ratio of particle density to gas density. The equation of translational motion of a particle can be written as follows [16]:

$$m\frac{dv_i}{dt} = -\frac{\pi}{6}d_i^3 \nabla P + f_d + m_i g \tag{7}$$

$$f_d = \left(\frac{1}{16}\right) C_{d0,i} \rho_g \pi d_i^2 |u_{gi} - v_i| (u_{gi} - v_i) \varepsilon_g^{-\delta} \tag{8}$$

where the drag force coefficient $C_{d0,i}$ is written as

$$C_{d0,i} = \left(0.63 + \frac{4.8}{Re_{p,i}^{0.5}}\right)^2 \tag{9}$$

$$Re_{p,i} = \rho_g d_i \frac{|u_{gi} - v_i|}{\mu_g} \tag{10}$$

$$\delta = 3.7 - 0.65 \ \exp\left[-\frac{(1.5 - \log_{10} Re_{p,i})^2}{2}\right] \tag{11}$$

The equation of rotational motion of a particle is written as

$$\frac{m_i d_i^2}{10}\frac{d\omega_i}{dt} = \frac{\rho_s d_i^2}{64}\left(\frac{6.45}{Re_\omega} + \frac{32.1}{Re_\omega}\right)|\omega_i|\omega_i \tag{12}$$

where $Re_\omega = d_i^2 \rho_g |\omega| / (4\mu_g)$.

2.3. Particle collision dynamics

The changes of velocity after a collision between two particles are subject to the equations [9,15,16]:

$$m_i(v_{i,1} - v_{i,0}) = J \tag{13}$$

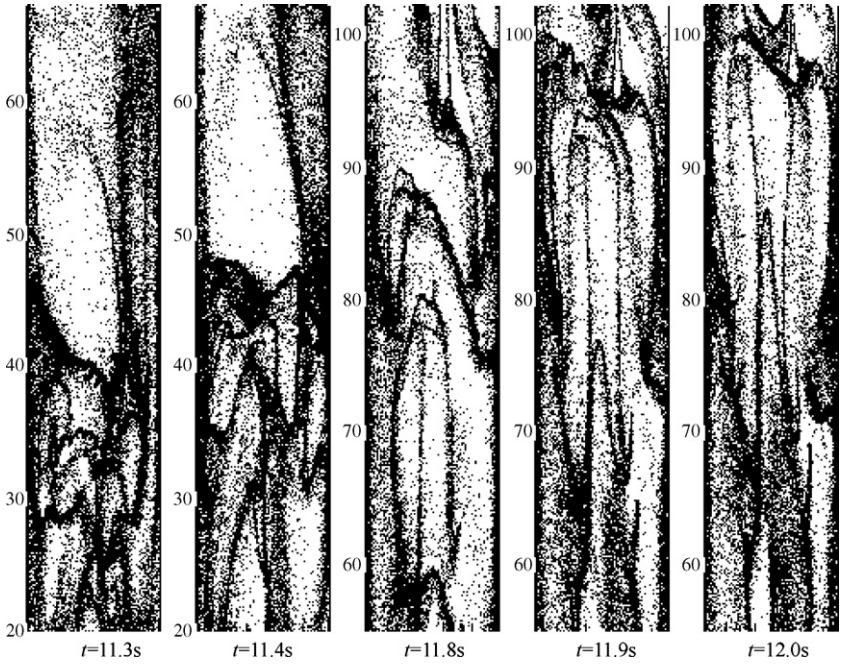

Fig. 3. Motions of clusters in the riser (first two images: y = 20–67 cm, last three images: y = 55–102 cm).

$$m_j(v_{j,1} - v_{j,0}) = J \tag{14}$$

$$\frac{m_i d_i^2}{4}(\omega_{i,1} - \omega_{i,0}) = n \times J \tag{15}$$

$$\frac{m_j d_j^2}{4}(\omega_{j,1} - \omega_{j,0}) = -n \times J \tag{16}$$

where $v_{i,0}$ and $v_{j,0}$ represent the pre-collisional velocities of particle i and particle j, respectively. $v_{i,1}$ and $v_{j,1}$ represent the post-collisional velocities of particle i and particle j, respectively. n is the normal unit vector between particles i and j. The relative velocity between the two colliding particles is defined as

$$v_{ij} = (v_{i,c} - v_{j,c}) \tag{17}$$

Table 1
Parameters used in the simulation.

Particle shape	Sphere	Solid flux	59 kg/m^2 s
Particle diameter	0.126 (mm)	Height of riser	1 (m)
Particle density	2400 (kg/m^3)	Width of riser	0.08 (m)
Particle inlet velocity	0.0 (m/s)	Superficial gas velocity	1.5 (m/s)
Restitution coefficient	0.9	Gas viscosity	1.5×10^{-5}(Pa s)
Coefficient of restitution between particle and wall	0.8	Gas density	1.2 (kg/m^3)
Tangential restitution coefficient	0.3	Grid number	20×25
Friction coefficient	0.1	Subgrid number	40×200

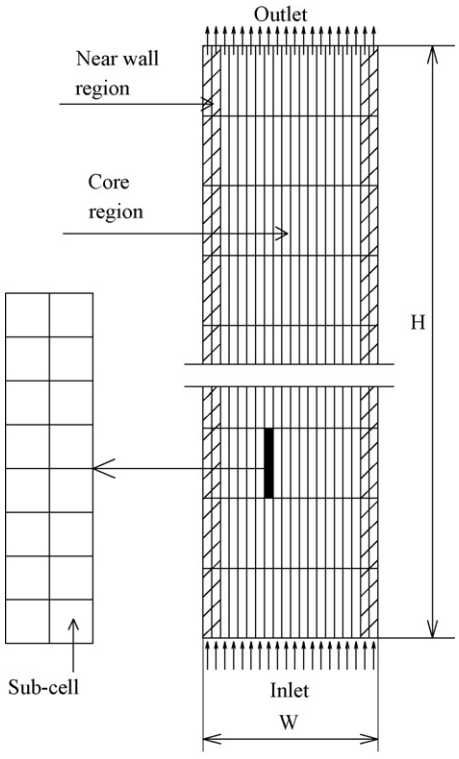

Fig. 2. Grid arrangement for simulation in the two-dimensional riser.

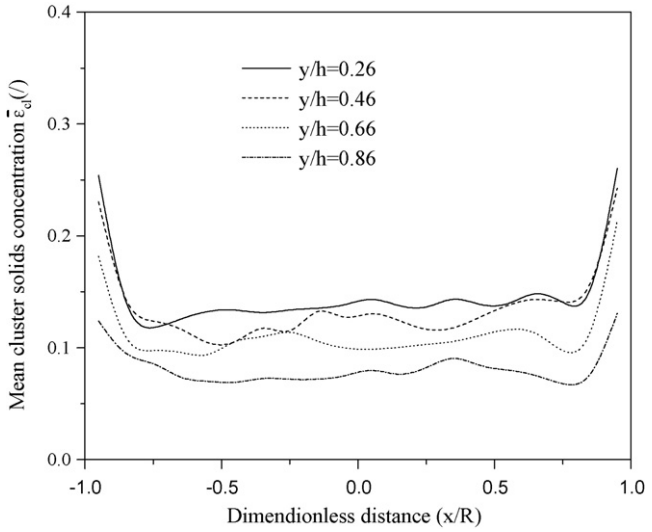

Fig. 4. Distribution of mean solid concentration of clusters.

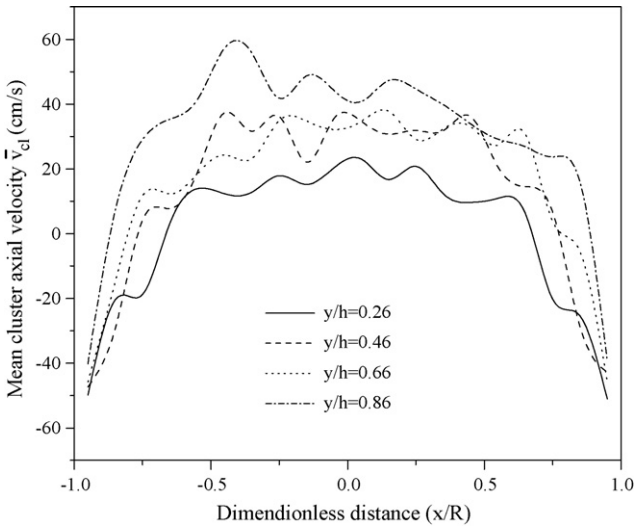

Fig. 5. Distribution of mean axial velocities of clusters.

The normal and tangential components of the impulse vector calculated by coefficient of restitution e and friction coefficient μ_f are written as

$$J_n = -\frac{(1+e)m_i m_j}{(m_i+m_j)}(v_{ij,0}\cdot n) \tag{18}$$

$$J_t = -\mu_f J_n \tag{19}$$

The total impulse vector is defined as

$$J = J_n n + J_t t \tag{20}$$

$$t = \frac{v_{ij,0} - n(v_{ij,0}\times n)}{\left|v_{ij,0} - n(v_{ij,0}\times n)\right|} \tag{21}$$

2.4. DSMC method

The DSMC method is widely used in the simulation of rarefied gas for handling collisions between gas molecules [17]. In the DSMC method, Colliding pair is found through the theory of collision probability instead of using particle trajectories. So significant saving in computation time and memory can be made and the number of simulated particles almost has not limitation. Detailed introduction of DSMC method is shown in our previous paper [18].

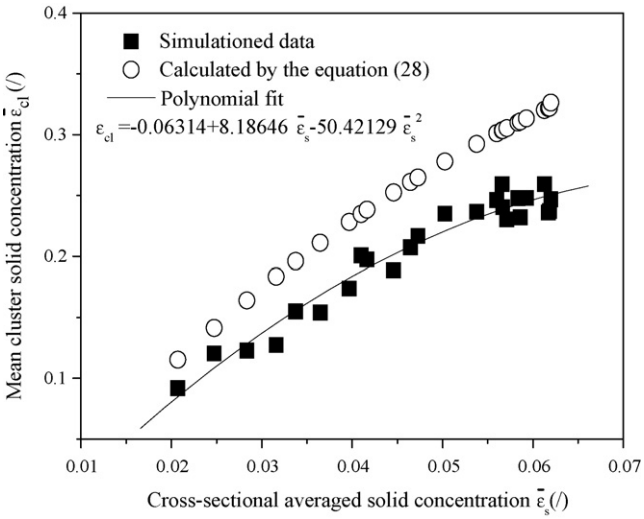

Fig. 6. Mean solid concentration of near wall clusters vs. cross-sectional averaged solid concentration.

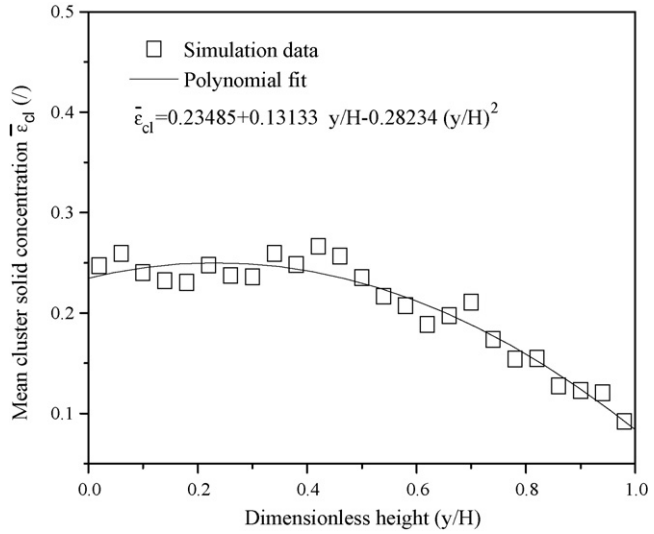

Fig. 7. Distribution of mean solid concentration of near wall clusters along the height of riser.

3. The extended method of identification of clusters

In order to obtain quantitative characteristics of cluster flow in a riser, one first needs a systematic criterion for identification of clusters. Soong et al. [19] proposed the following three necessary guidelines. (1) The solid concentration in a cluster must be significantly above the time-averaged solid concentration at the given local position and operating condition. (2) This perturbation in solid concentration due to clusters must be greater than random background fluctuations of solid concentration. (3) This concentration perturbation should be sensed for sampling volume with characteristic length scale greater than one to two orders of particle diameter. Being consistent with these guidelines, Sharma et al. [3] proposed a criterion that the local instantaneous solid concentration for a cluster must be greater than the time-averaged concentration by at least two times the standard deviation 2σ. In this study, we extend this method to investigate the velocity and the solid concentration of clusters. Principle is shown in Fig. 1. The starting time t_{i1} and end-

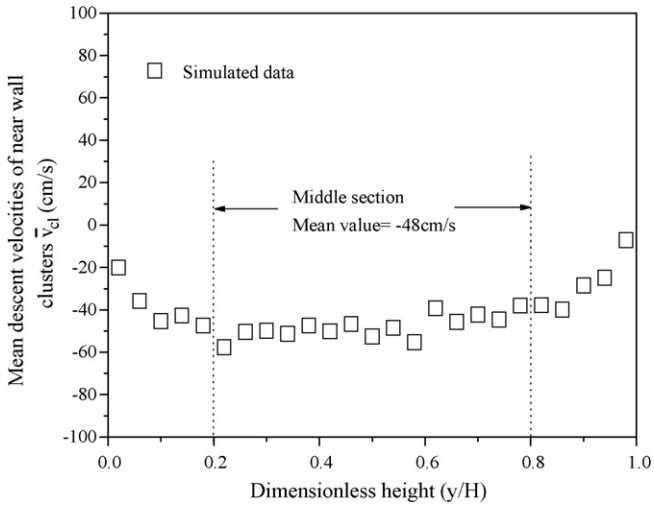

Fig. 8. Distribution of mean descent velocities of near wall clusters along the height of riser.

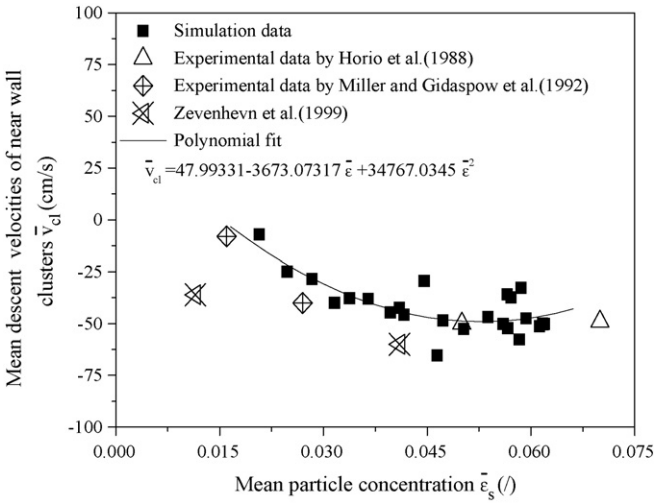

Fig. 9. Mean cluster descent velocities vs. mean solid concentration.

ing time t_{i2} of cluster i can be determined by criteria proposed by Sharma et al. The cluster duration time is defended as $\tau_i = t_{i1} - t_{i2}$. The instantaneous velocity v_i and solid concentration ε_i of cluster i are

$$X_i = \frac{\sum_{j=1}^{m} X_{s,j}}{m} \tag{22}$$

where $m = \tau_{cl,i}/\Delta t$, Δt is the time step. X represents either velocity v or solid concentration ε.

The time-averaged cluster solid concentration ε_{cl} and velocity v_{cl} in a computational cell P can be calculated as

$$X_{cl,p} = \frac{\sum_{i=1}^{N}(X_i \times \tau_i)}{\sum_{i=1}^{N}\tau_i} \tag{23}$$

where N is the number of cluster occurrence in the computational cell during the simulation.

The time-averaged cluster frequency and existence time fraction in a computational cell P, $\lambda_{cl,p}$ and $F_{cl,p}$, can be calculated as

$$\lambda_{cl,p} = \frac{N}{T} \tag{24}$$

$$F_{cl,p} = \frac{\sum_{i=1}^{N}\tau_i}{T} \tag{25}$$

where T is the total simulation time.

The mean (cross-sectional averaged) values can be calculated as

$$\bar{Y}_{cl} = \frac{\sum_{p=1}^{M} Y_{cl,p}}{M} \tag{26}$$

where M is the number of cells (near wall or in the core of riser) in certain cross-section. Y can represent ε, v, λ and F.

4. Initial and boundary conditions

In order to the calculation of the force acting on a suspended particle, local averaged values of pressure, porosity and velocity of gas at the position of the particle are obtained by the area weighted averaging technique. The details are described in the paper by Wang et al. [18]. For each cell of the computational domain, porosity can be calculated on the basis of the area occupied by the particles in the cell. However, the 2D porosity is inconsistent with the applied empiricism in the calculation of the drag force exerted on a particle and of the interfacial friction, since the relevant correlations are from 3D systems. In order to be more consistent, we used a 3D porosity $\varepsilon_{g,3D}$ as [16]

$$\varepsilon_{g,3D} = 1 - \frac{2}{\sqrt{\pi\sqrt{3}}}(1 - \varepsilon_{g,2D})^{3/2} \tag{27}$$

Fig. 2 shows the two-dimensional riser section used in the simulation. The computational parameters and particle features are listed in Table 1. Initially, the bed is assumed to be empty. The velocities of gas and particles were set at zero in the riser. Inlet gas pressure, gas velocity and particle velocity are given. Uniform bottom-inlet conditions are assumed. A no-slip condition is used for gas phase at the walls. The rotational velocity of particle is zero at the walls.

5. Results and discussion

Fig. 3 shows the snapshots of particle and clusters in the riser. Firstly, the core-annulus flow structure can be observed with a denser zone close to the walls and a dilute zone in the core of riser. The solid concentration at the lower part of riser is higher than that of upper part. Secondly, the clusters with a local high solid concentration are observed not only at the wall region but also in the core of riser. The snapshots show the representative cluster structure in the riser. In the core of riser, the V-shaped and inverse V-shaped clusters can be observed and the clusters travel upward or downward. The clusters near the wall flow downward all the time. The formation, motion and breaking of clusters appear continuously.

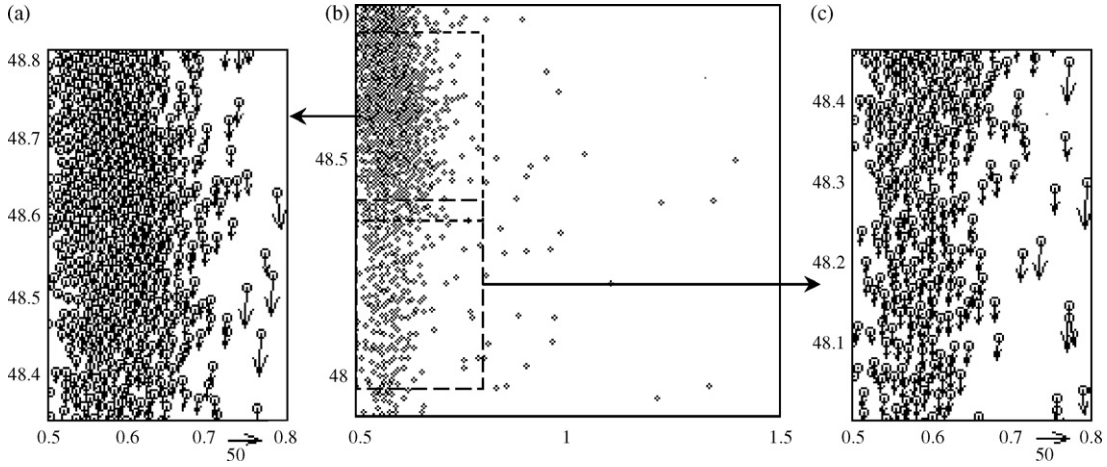

Fig. 10. Motion of a cluster near at the wall of riser ((a) y = 47.9–48.8 cm, x = 0.5–1.5 cm; (b) y = 48.35–48.8 cm, x = 0.5–0.8 cm; (c) y = 48–48.46 cm, x = 0.5–0.8 cm).

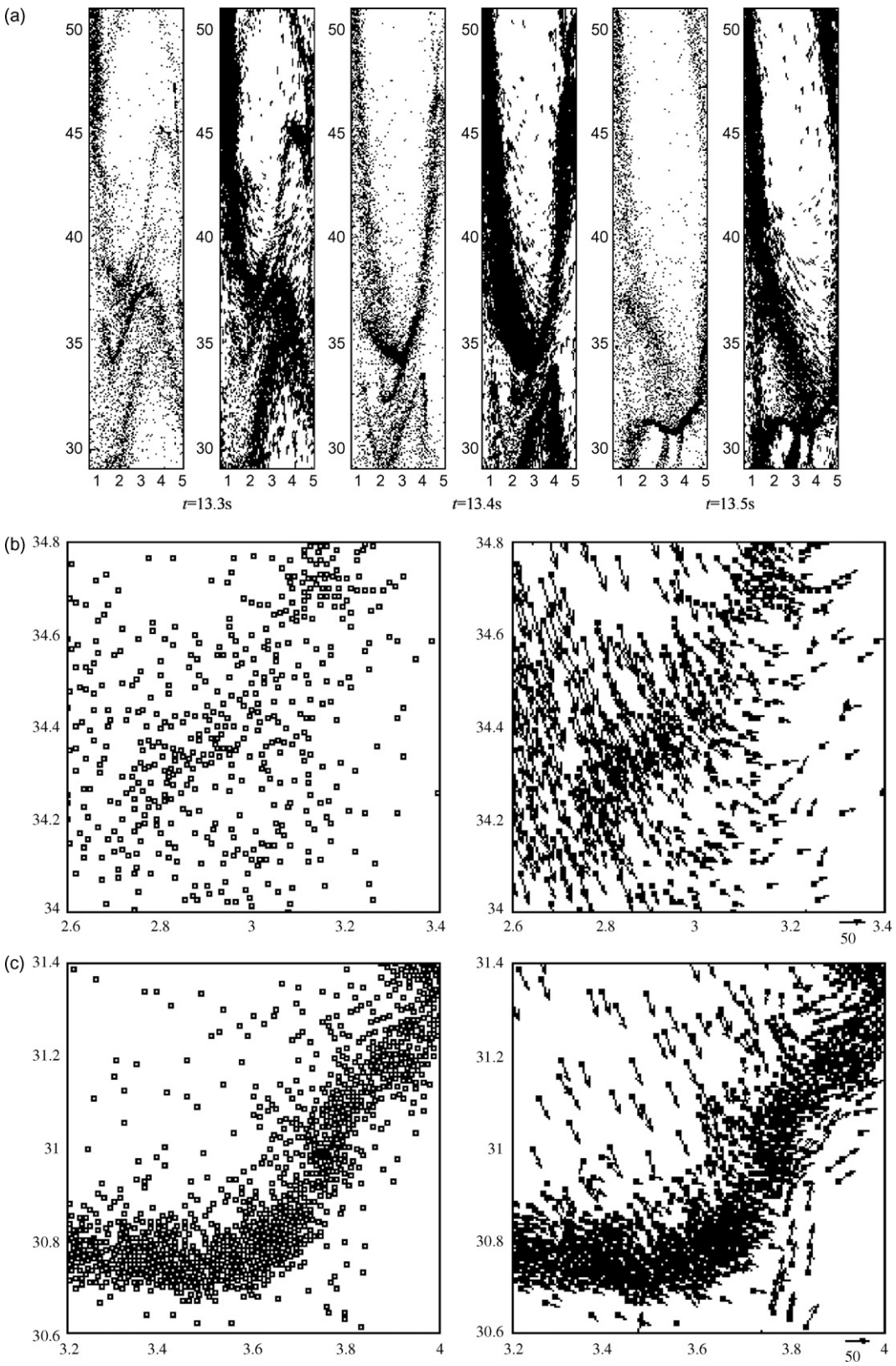

Fig. 11. The process of a cluster formation and traveling near the wall of riser (a) left: concentration, right: velocity, $x = 0.5–5$ cm, $y = 29–51$ cm; (b) ($t = 13.4$ s; left: concentration, right: velocity; $x = 2.6–3.4$ cm, $y = 34–34.8$ cm; (c) $t = 13.5$ s; left: concentration, right: velocity; $x = 3.2–4$ cm, $y = 30.6–31.4$ cm.

The size, shape, solid concentration and velocities of clusters vary continuously during their flow process.

Fig. 4 shows the distribution of mean solid concentration of cluster at the different height of riser. From the Fig. 4, we can see that the mean solid concentration of cluster near the wall is higher than that in the core. At the same time, the mean solid concentration of cluster decreases along the height of riser. Fig. 5 shows the distribution of mean axial velocities of clusters at the different height of riser.

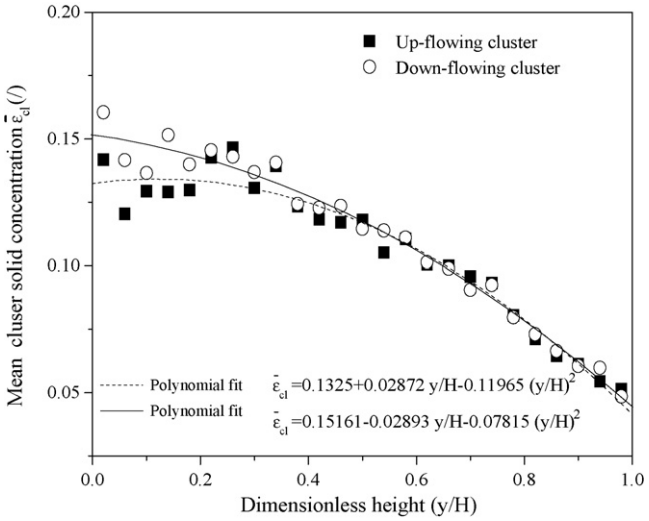

Fig. 12. Cross-sectional averaged cluster solid concentration along the height of riser.

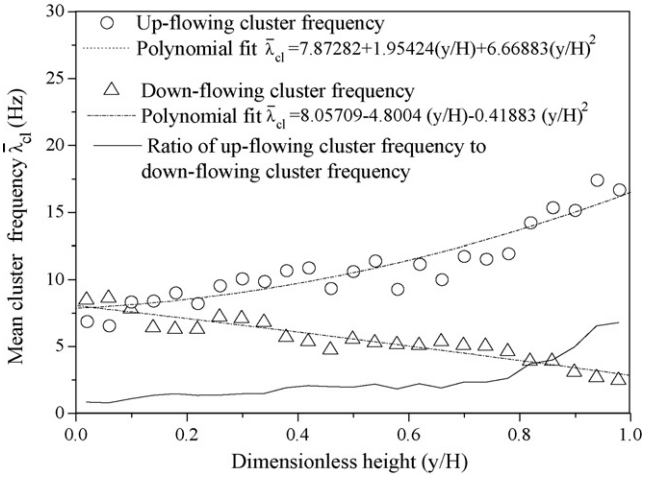

Fig. 14. Cross-sectional average cluster frequency along the height of riser.

The mean axial velocities of clusters near the wall are negative. This means that most of the clusters near the wall flow downward. And the cluster descent velocities lie within a small range from −55 cm/s to −40 cm/s. The mean axial velocities of clusters in the core are positive. This means that the main flow tendency of clusters in the core of riser is upward, although the up-flowing and down-flowing clusters coexist there. At the same time, the mean axial velocities of clusters in the core increase along the height of riser.

In this paper, the near wall cluster is defined as the cluster flowing in the near wall region, as shown in Fig. 2. Many experiments have been performed to study the mean solid concentration of clusters near the wall of riser. Their experimental data have confirmed that there exists a relationship between the solid concentration of near wall clusters and the cross-sectional averaged solid concentration of riser. The experimental data are correlated by the equation proposed by Harris et al. [20]. The equation is defined as:

$$\bar{\varepsilon}_{cl} = \frac{0.58\bar{\varepsilon}_s^{1.48}}{0.013 + \bar{\varepsilon}_s^{1.48}} \tag{28}$$

where $\bar{\varepsilon}_s$ is the cross-sectional averaged solid concentration.

Fig. 6 shows the distribution of mean solid concentration of near wall clusters as a function of cross-sectional solid concentration. The data calculated by the Eq. (28) are shown in the figure too. From the Fig. 6, we see that the mean solid concentration of near wall clusters increase with the increase of cross-sectional averaged solid concentration. The tendency of simulated results is in agreement with the calculated data by the Eq. (28), although the simulated results are little smaller. This discrepancy between the simulated results and experimental data is most likely due to the criterion used to identify the cluster. Fig. 7 shows the distribution of mean solid concentration of near wall clusters along the height of riser. The mean solid concentration of near wall clusters has no obvious change in the lower part of riser. But in the middle and upper parts of riser, the mean solid concentration of near wall clusters decreases along the height of riser.

The descent velocities of clusters near the wall have been studied and reported by many investigators. Fig. 8 shows the variation of the mean axial velocities of near wall clusters along the height of riser. From Fig. 8, we can see that the mean axial velocities of near wall clusters are negative. This means the near wall clusters always travel downward. The mean descent velocities of near wall clusters increase at the lower part of riser ($y/H < 0.2$) and appear to keep a constant of −48 cm/s in the middle part of riser ($y/H = 0.2$–0.8) and decrease again at the upper part ($y/H > 0.8$) of riser. A lot of experimental data have confirmed that the axial velocity of near wall cluster appears to be relative constant and insensitive to changes in

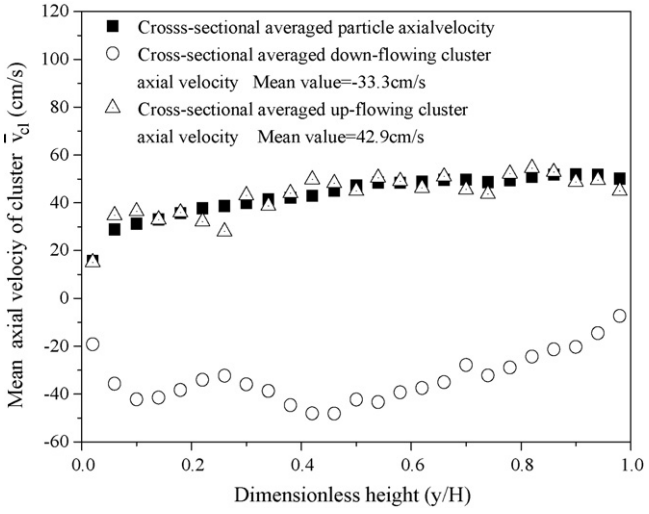

Fig. 13. Cross-sectional averaged cluster axial velocity along the height of riser.

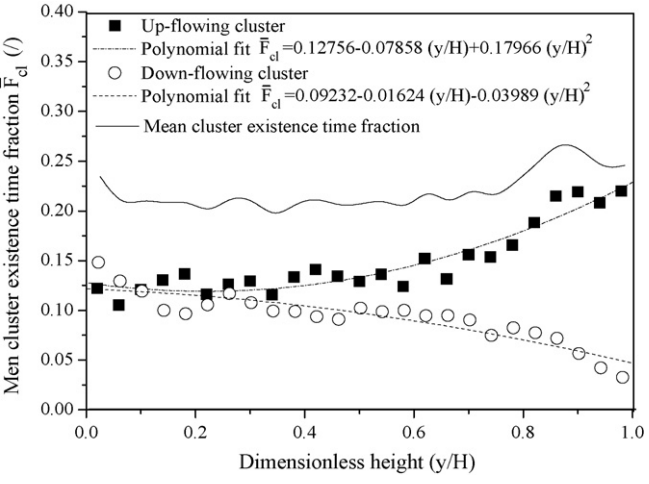

Fig. 15. Cross-sectional averaged cluster existence time fraction along the height of riser.

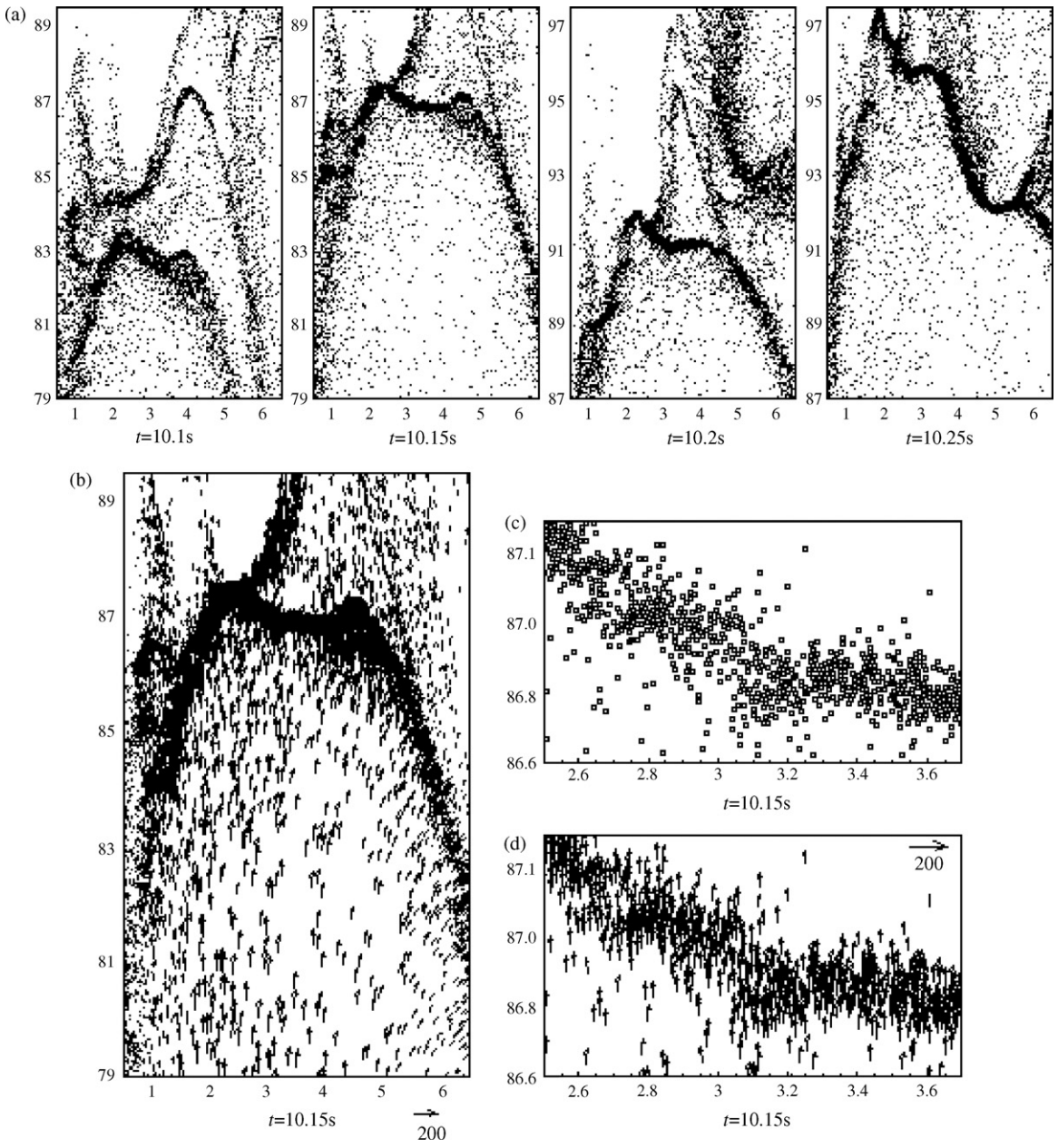

Fig. 16. Motions of up-flowing cluster in the core of riser. (a) $x = 0.5–6.5$, $y = 79–89.5$ cm/$y = 87–97.5$ cm; (b) $t = 10.15$ s, $x = 0.5–6.5$ cm, $y = 79–89.5$ cm; (c and d) $t = 10.15$ s, $x = 2.5–3.7$ cm, $y = 86.6–87.3$ cm.

solid concentration and other operating conditions and the velocity usually lies within the range −0.5 m/s to 2 m/s [21]. The measure positions in these experiments are usually located in the middle part of riser. At the lower part, on the one hand, the mean solid concentration is so high that the clusters have no enough free space to move, on the other hand, the gas phase prevents the clusters falling. So the cluster descent velocity decreases. At the upper part, the solid concentration and the thickness of near wall falling particle film decrease along the height of riser, so the positive velocities of some up-flowing particles and clusters in the computational cell will be added in the calculation of cluster decent velocity base on the cluster identification method used in this paper which will averaging all the particles' velocities in the cell. So the cluster descent velocity decreases. Fig. 9 shows the variation of mean descent velocity of near wall clusters as a function of the cross-sectional averaged solid concentration. The reported relative experimental data [22–24] are also showed in the figure. From Fig. 9, we can see that the descent velocity of near wall clusters increase with the increase of cross-sectional solid concentration and the simulated results are close to the experimental data.

Cluster near the wall of riser have been observed to form, descend, break-up, travel laterally from the annulus to the core and then be re-entrained in the upward flowing core in the experimental study by Horio et al. [25]. In this study, we study this micro-scale flow characteristic by means of discrete particle method. Fig. 10b shows a snapshot of a down-flowing cluster at the wall. Fig. 10a and c show the velocities of particles in the upper and lower sections of this cluster. We can see that in this case the thickness of solid film formed by the falling clusters and discrete particles is smaller than the criterion proposed by Davision et al. who think the mean thickness of falling film is 0.05 times the radius of riser [26]. The particles in it fall with the same descent velocities and almost have no radial velocities. So the particles can only flow vertically toward the bottom. Comparing the Fig. 10a with Fig. 10c, we can see that a

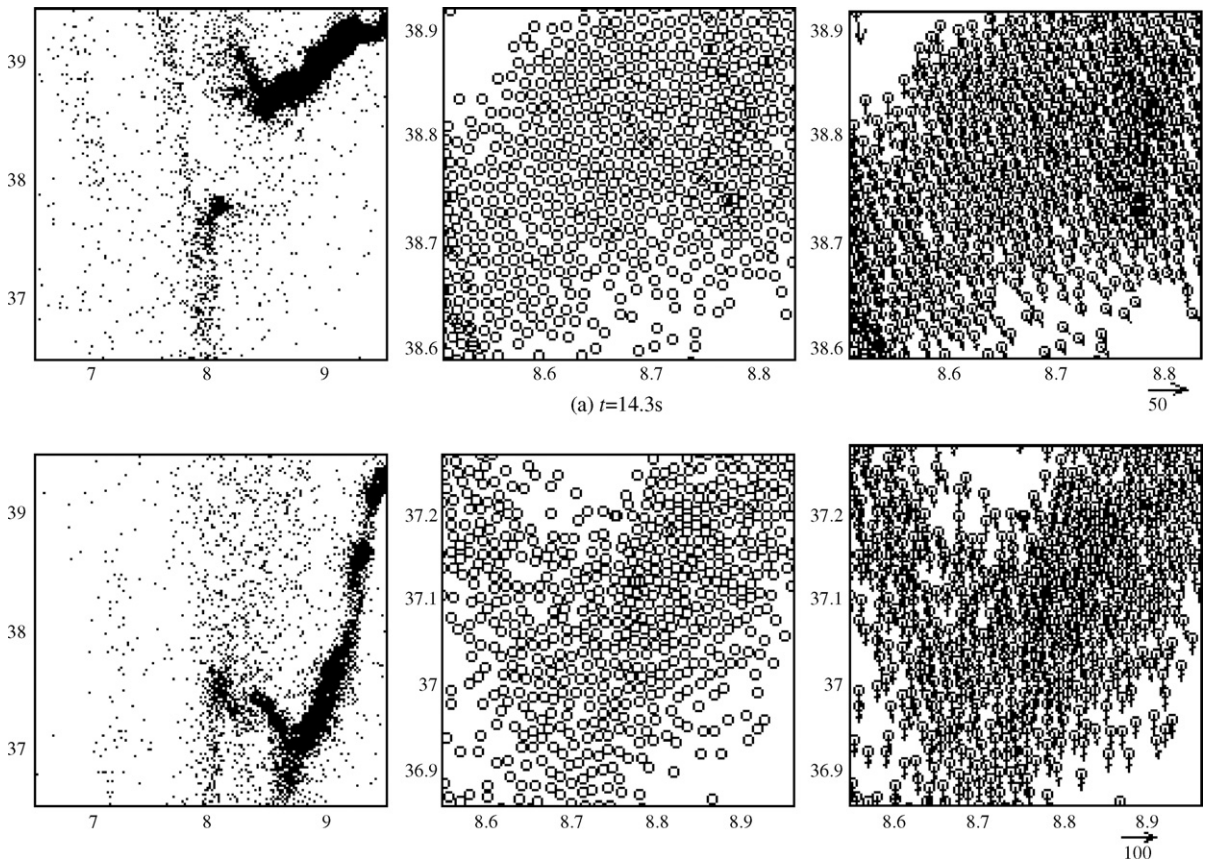

Fig. 17. The down-flowing cluster behavior (from left to right: particle concentration, $x = 6.5–9.5$ cm, $y = 36.5–39.5$ cm; local particle concentration; particle velocity, $x = 8.54–8.96$ cm, $y = 36.8–37.3$ cm).

near wall falling cluster consist of an upper dense section in which the particles have smaller descent velocities and a lower little dilute section in which the particles have relatively larger descent velocities. This velocity distribution characteristic may be attributed to the drag force model used in present study. Fig. 11a shows the process of a near wall cluster formation and traveling from the wall to the core region under the effect of upgoing gas. Fig. 11b and c show the solid concentration and particle velocities in the cluster at 13.4 s and 13.5 s, respectively. From Fig. 11a, we can see that if the local falling solid film is thick enough the upgoing gas will have a significant effect on the particles in it, especially on the particles on the edge of the solid film. At 13.3 s, the descending particles are hindered by the upgoing air and their descent velocities decrease. Particles begin to aggregate at this local position, which will result in the local solid concentration increase and a dense cluster begin to form. From Fig. 11b and c, we can see that during the cluster formation process particles in it can get radial velocities gradually and the developing cluster starts to travel toward the core of riser. The simulated zones shown in the Fig. 11b and c are in the same size, so we can compare the solid concentration between them. It is obvious that the solid concentration of cluster at 13.5 s is much higher than that at 13.4 s. This means that the solid concentration of cluster increase during its formation process. At the same time, from the Fig. 11c, we see that the cluster grows up by capturing the descending particles above it continuously. The lateral velocities of particles in cluster increase, on the contrary their axial velocities decrease.

It is well known that the up-flowing and down-flowing clusters coexist in the core of riser. Fig. 12 shows the distribution of cross-sectional averaged solid concentration of clusters in the core region along the height of riser. From Fig. 12, we can see that at the lower part of riser the cross-sectional averaged solid concentration of down-flowing cluster is slightly larger than that of up-flowing cluster. In the middle and upper parts of riser they are almost equal to each other. Along the height of riser the cross-sectional averaged solid concentration of both kind clusters decrease. Fig. 13 shows the distribution of cross-sectional averaged axial velocities of up-flowing and down-flowing clusters in the core region along the height of riser. From Fig. 13, we can see that the cross-sectional averaged axial velocity of up-flowing cluster fluctuate around the cross-sectional averaged solid velocity, and there always exists a difference between them at an arbitrary height. This means that the up-flowing cluster does not flow with discrete particles isochronously and should flow in the decelerated and accelerated states continuously in the vertical direction. The cross-sectional averaged axial velocities of down-flowing clusters lie within a wide range from −50 cm/s to −20 cm/s. The mean value is −33.3 cm/s and smaller than that of cluster near the walls. The cross-sectional averaged axial velocities of down-flowing clusters in the core decrease along the height of middle and upper parts of riser. So the velocity distribution of cluster is different with that near the wall. This is because that the gas phase has a great effect on the flow behavior of cluster in the core of riser. The cluster frequency is the cluster occurrence number per second at a local position and the mean cluster frequency is defended as the cross-sectional averaged cluster frequency at certain height. Cluster existence time fraction is the ratio of the cluster occurrence time to total simulation time at a local position and the mean cluster existence time fraction is defended as the cross-sectional averaged cluster time fraction at certain height. The mean cluster frequency and existence time fraction can be calculated from Eqs. (24)–(26). Fig. 14 shows the distributions of the cross-sectional averaged occurrence

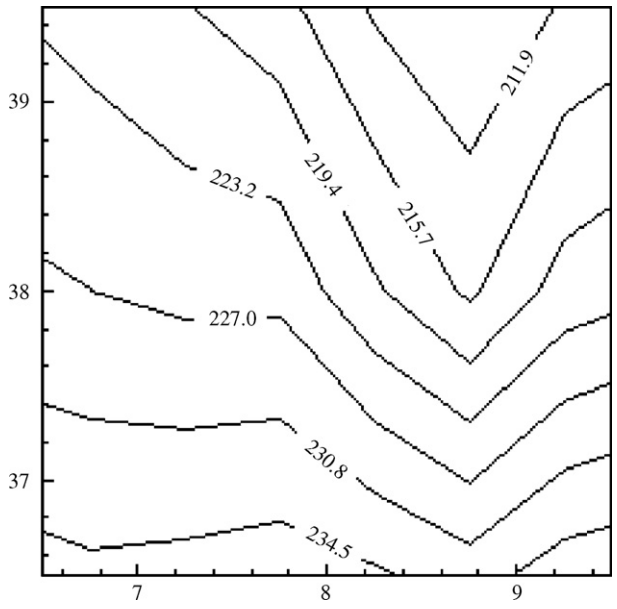

Fig. 18. Pressure profile of a down-flowing cluster (t = 14.35 s, unit is Pascal).

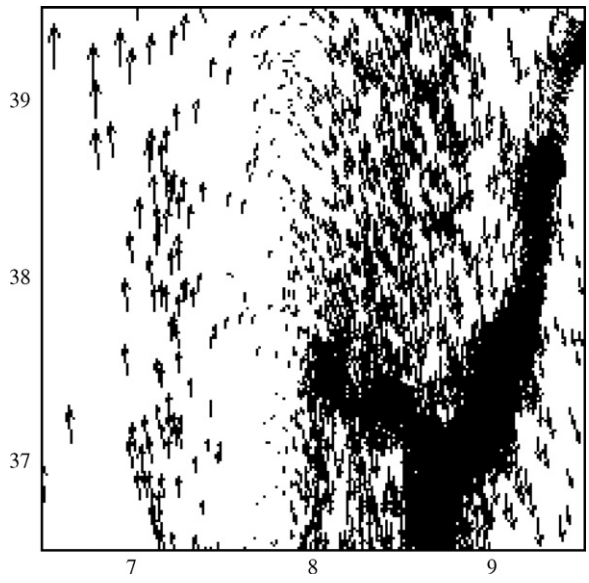

Fig. 19. Velocities of particles near the tails of a down-flowing cluster (t = 14.35 s).

frequencies of up-flowing and down-flowing clusters in the core along the height of riser. The ratio of up-flowing cluster frequency to down-flowing cluster frequency is also shown in the figure. We see that the up-flowing cluster frequency increase along the height of riser, while that of down-flowing cluster decrease. The ratio of cluster frequency increases along the height of riser. In the upper part of riser ($y/H > 0.8$), the ratio increases sharply, which means that clusters tend to flow upward. Simulated results by Wang and Li et al. [27] confirmed this flow tendency. Fig. 15 shows the distribution of cross-sectional averaged existence time fraction of up-flowing and down-flowing clusters in the core along the height of riser. We can see that the up-flowing cluster existence time fraction increase along the height of riser, while the down-flowing cluster decrease. The mean cluster existence time fraction defined as the sum of both kind clusters' existence time fraction is also shown in the figure. In the middle part of riser the cluster existence time fraction appears to keep constant and the mean value is 0.22. Experimental result by Sharma et al. [3] showed that the bed-averaged cluster existence time fraction always lies within the range of 0.16–0.18 and have no relationship with the operating condition. From above analysis, we see that in the core up-flowing and down-flowing clusters' frequencies and existence time fractions are different and exhibit relationships shown in Figs. 14 and 15. The most likely explanation for this distribution is that when clusters flow upward in the core and their solid concentration and velocities vary continuously, which will lead to the variation of the interaction force between the two phases. So under some conditions, in some periods of time, some clusters may turn downward temporarily and then recover flow upward. From Figs. 14 and 15, we know that this downward flow frequency and duration decrease along the height of riser.

Fig. 16a shows snapshots of a typical up-flowing cluster in the upper part of riser. We can see that the up-flowing cluster exhibits a horseshoe shape ahead upwards leaving two roughly symmetrical tails. This is in good agreement with the experimental findings by Van Den Moortel et al. [2]. From the figures, we see that the solid concentration in the head zone of the up-flowing cluster is higher than that in the tails. The cluster is accelerated from 10.1 s to 10.2 s. The structure of cluster is damaged by the gas and colliding with another down-flowing cluster at 10.15 s. The duration time of this cluster is about 0.15 s. Fig. 16b shows the velocity of particles at 10.15 s. Fig. 16c and d show the particle concentration and velocity in the head of cluster at 10.15 s, respectively. From these figures, we see that the velocity of particle in the head is higher than that of particle in the tails and than that of isolated particle in front of the cluster. So from the above analysis we can see that on the one hand the up-flowing cluster capture isolated particles in front of it, on the other hand it reject old particles from its tails during its motion process continuously.

Fig. 17 shows snapshots of a down-flowing cluster in the core of riser at 14.3 s and 14.35 s, respectively. At 14.3 s, the axial velocity of cluster is smaller, and the cluster exhibits a strand shape. From 14.3 s to 14.35 s, the cluster is accelerated in the axial direction and the V-shaped cluster instead of the strand-shaped cluster. Although not shown in the paper, the down-flowing clusters in present simulation almost exhibit this structure. So we can see that the cluster shape is closely related with the cluster velocity and flow direction. Fig. 18 shows the pressure profile near this down-flowing cluster at 14.35 s. The pressure shown in the figure is gage pressure. From Fig. 18, we can see that there exists an obvious low-pressure zone between the tails of this down-flowing cluster. Fig. 19 shows the particle velocities at 14.35 s. Form Fig. 19, we can see that the discrete particles near the tails of cluster can be dragged into the low-pressure zone and flow downward. This phenomenon has also been reported by some investigators who perform the circulating fluidized bed experiment.

6. Conclusion

The Euler–Lagrangian approach is used to model hydrodynamics of gas and particles phases in the CFBs. The LES is used to model gas turbulence. Particle collision is modeled by means of the DSMC method. An extended cluster identification method is used to investigate the distributions of solid concentration and velocity of cluster near the wall and in the core of riser. Simulated results show that in the core region, the up-flowing cluster exhibits a horseshoe shape with a dense head and both dilute tails and flow in the decelerated and accelerated states continuously. The down-flowing cluster exhibits an inversed-V shape. There exists a low-pressure zone between their tails and the particles near it may be dragged into it. The ratio of up-flowing cluster frequency to down-flowing cluster frequency increases along the height of riser. In the near wall region, the clusters descend velocity seems to keep constant. The descent particles and clusters form a falling particle film. If the local

solid film is thick enough, the particles in it can be hindered by the upgoing gas and form a new cluster that will be entrained into the core of rise under the effect of gas phase. Simulation results show a reasonable agreement with previous experimental findings.

Acknowledgement

This work was supported by National Key Project of Science and Technology of China (No. 2006BAA03B01-10).

References

[1] X. Liu, S. Gao, J. Li, Characterizing particle clustering behavior by PDPA measurement for dilute gas–solid flow, Chem. Eng. J. 108 (2005) 193–202.
[2] T. Van den Moortel, E. Azario, R. Santini, Tadrist experimental analysis of the gas-particle flow in a circulating fluidized bed using a phase Doppler particle analyzer, Chem. Eng. Sci. 53 (1998) 1883–1899.
[3] A.K. Sharma, K. Tuzla, J. Matsen, J.C. Chen, Parametric effects of particle size and gas velocity on cluster characteristics in fast fluidized beds, Powder Technol. 111 (2000) 114–122.
[4] S.V. Manyele, J.H. Parssinen, J.X. Zhu, Characterizing particle aggregates in a high-density and high-flux CFB riser, Chem. Eng. J. 88 (2002) 151–161.
[5] Y.P. Tsuo, D. Gidaspow, Computation of flow patterns in circulating fluidized beds, AIChE J. 36 (1990) 885–896.
[6] H. Lu, Q. Sun, Y. He, Y. Sun, D. Jianmin, X. Li, Numerical study of particle flow in risers with cluster-based approach, Chem. Eng. Sci. 60 (2005) 6757–6767.
[7] Y. Tsuji, T. Tanaka, S. Yonemura, Cluster patterns in circulating fluidize beds predicted by numerical simulation (discrete particle model versus two-fluid model), Powder Technol. 95 (1998) 254–264.
[8] J. Ouyang, J. Li, Discrete simulations of heterogeneous structure and dynamic behavior in gas–solid fluidization, Chem. Eng. Sci. (1999) 5427–5440.
[9] E. Helland, R. Occelli, L. Tadrist, Computational study of fluctuating motions and cluster structures in gas-particle flows, Int. J. Multiphase Flow 28 (2002) 199–223.
[10] E. Helland, H. Bournot, R. Occelli, L. Tadrist, Drag reduction and cluster formation in a circulating fluidized bed, Chem. Eng. Sci. 62 (2007) 148–158.
[11] S. Yonemura, T. Tanaka, Cluster formation in gas–solid flow predicted by DSMC method, Gas–Solid Flows 166 (1993) 303–309.
[12] T. Tanaka, S. Yonemura, Kiribayashi, Y. Tsuji, Effects of particle properties on the structure of clusters, America Society of Mechanical Engineers, Fluids Eng. Div. 228 (1995) 297–302.
[13] T. Tanaka, S. Yonemura, Kiribayashi, Y. Tsuji, Cluster formation and particle-induced instability in gas–solid flows predicted by the DSMC method, Int. J. JSME 39 (1996) 239–245.
[14] D. Gidaspow, Multiphase Flow and Fluidization: Continuum and Kinetic Theory Descriptions, Academic Press, Boston, 1994.
[15] S. Yuu, T. Ueno, T. Umekage, Numerical simulation of the high Reynolds number slit nozzle gas-particle jet using subgrid-scale coupling large eddy simulation, Chem. Eng. Sci. 56 (2001) 4293–4307.
[16] B.P.B. Hoomans, J.A.M. Kuipers, W.J.W. Briels, P.M. Van Swaaij, Discrete particle simulation of bubble and slug formation in a two-dimensional gas-fluidized bed: a hard-sphere approach, Chem. Eng. Sci. 51 (1996) 99–118.
[17] G.A. Bird, Molecular Gas Dynamics and the Direct Simulation of Gas flows, CRC Press, Oxford, 1994.
[18] S. Wang, H. Liu, H. Lu, W. Liu, D. Jiamin, W. Li, Flow behavior of clusters in a riser simulated by direct simulation Monte Carlo method, Chem. Eng. J. 106 (2005) 197–211.
[19] C.H. Soong, K. Tuzla, J.C. Chen, Experimental determination of clusters size and velocity in circulating fluidizeds, in: J.F. Large, C. Laguerie (Eds.), Fluidization VIII, Engineering Foundation, New York, 1995, pp. 219–227.
[20] A.T. Harris, J.F. Davidson, R.B. Thorpe, The prediction of particle cluster properties in the near wall region of a vertical riser, Powder Technol. 127 (2002) 128–143.
[21] M. Horio, K. Morishita, O. Tachibana, N. Murata, Solid distribution and movement in circulating fluidized beds, in: P. Basu, J.F. Large (Eds.), Circulating Fluidized Bed Technology II, Pergamon, Oxford, 1998, pp. 147–154.
[22] A. Miller, D. Gidaspow, Dense vertical gas–solid flow in apipe, AIChE J. 38 (1992) 1801–1815.
[23] R. Zevenhoven, Ner wall particle velocity and concentration measurements in circulating fluidized beds in relation to heat transfer, Proceedings of the 15th International Conference on Fluidized Bed Combuston, Savannah, GA, American Society of Mechanical Engineers, 1999, Paper No.FBC99-0097.
[24] Hongzhong Li, Qingshan Zhu, Hua Liu, Yufeng Zhou, The cluster size distribution and motion behavior in a fast fluidized bed, Powder Technol. 84 (1995) 241–246.
[25] M. Horio, H. Kuroki, Three-dimensional flow visualisation of dilutely dispersed solids in bubbling and circulating fluidised beds, Chem. Eng. Sci. 49 (1994) 2413–2421.
[26] J.F. Davidson, Circulating fluidized bed hydrodynamics, Powder Technol. 113 (2000) 249–260.
[27] W. Wang, J. Li, Simulation of gas–solid two-phase flow by multi-scale CFD approach—Extension of the EMMS model to the sub-grid level, Chem. Eng. Sci. 62 (2007) 208–231.